

# Offshore Underwater Image Restoration Using Reflection-Decomposition-Based Transmission Map Estimation

Miao Yang<sup>✉</sup>, Member, IEEE, Arcot Sowmya, Member, IEEE, ZhiQiang Wei, and Bing Zheng

**Abstract**—A new restoration model for underwater images is presented, based on the dark channel reflection-illumination decomposition and local backscattering lighting estimation, to promote the clarity of edge detail and the colorfulness of the output image. For turbid offshore environments, a novel underwater image restoration method is further introduced by applying a statistical prior to the offshore attenuation coefficients. It is shown that the estimated transmission map with lighting-reflection decomposition, rather than dividing the dark channel by the maximal backscattering light as the other methods do, provides better clarity and color restoration. Detailed qualitative and quantitative analysis on hundreds of underwater images is performed, which demonstrates that the proposed method outperforms the state-of-the-art algorithms on the images taken in offshore water characterized by a heavy concentration of colored dissolved organic matter and total suspended matter, and is suitable for fast underwater processing.

**Index Terms**—Offshore, underwater image restoration, underwater imaging, underwater optical model.

## I. INTRODUCTION

UNDERWATER optical camera imaging is a necessary and conventional technology that is widely used due to its low cost and rich object information that can be obtained when compared with other imaging techniques. However, underwater image quality is highly degraded by the comprehensive light attenuation from inside optical properties in pure water, the solute in seawater (molecular scattering and absorption), and

suspended particles in water (particle scattering and absorption). The poor visibility and color cast caused by the effects of underwater imaging reduce the capability to extract valuable features from underwater images for further processing [1]. Therefore, restorations of the degraded underwater images are necessary for obtaining high-quality underwater images, which have been approached from several angles include the use of specialized hardware [2], stereo images [3], polarization filters [4], and dehazing algorithms [5]–[11]. As far as single underwater image enhancement methods are concerned, Iqbal *et al.* [6], [7] proposed the integrated color model and the unsupervised color-correction method. Fu *et al.* [8] constructed a color stretch based variational Retinex model on the luminance channel. Chiang and Chen [9] restored underwater images by combining a dehazing algorithm with wavelength compensation. Ancuti *et al.* [10], [12] enhanced the visual quality of underwater images and videos by using fusion principles. They proposed an improved white balance by red channel loss compensation before resorting to the conventional Gray-World [13]. Gamma correction and a highpass filter are adopted in the fusion process to obtain the final output [12]. However, at least three multiscale subimages have to be computed before fusion, and the underwater degradations may be due to varying causes, which violates the assumption that the green channel is always well preserved under water.

He *et al.* [14] proposed the dark channel prior (DCP), based upon the observation that haze-free images have at least one color channel with very low-intensity values, and therefore values in the dark channel of the hazy images could be attributed to the haze. This paper motivated many methods of underwater image restoration by the estimation of background lighting and transmission map [14]–[21]. Galdran *et al.* [15] proposed a red channel prior and estimated the ambient light from the pixel with the highest intensity in the red channel. Carlevaris-Bianco *et al.* [16] computed the dark channel image by the difference between the maxima in the red channel and the green-blue channel, and the background light was estimated as the highest intensity of the dark channel. Drews-Jr. *et al.* [17] also built on the DCP, and assumed that the dominated information included in an underwater image lay in the blue and green color channels. Peng *et al.* [18], [19] proposed a transmission estimation method by applying the information of image blurriness [18] and selected a single background intensity from the blurry regions [19]. They further improved the transmission

Manuscript received January 8, 2018; revised June 27, 2018 and November 21, 2018; accepted December 5, 2018. This work was supported in part by the National Natural Science Foundation under Grant 61601194, the “Six talent peaks” project in Jiangsu Province (No. DZXX-030), and in part by Lianyungang “521” funded project (2017-4), and “Haiyan” funded project (2017–8). This work was presented in part at the IEEE/MTS OCEANS Conference, Aberdeen, Scotland, June 19–22, 2017. (Corresponding author: Miao Yang.)

Associate Editor: J. Watson.

M. Yang was with the School of Computer Science and Engineering, University of New South Wales, Sydney, NSW 2052, Australia. She is now with the Department of Electronic and Engineering, Huaihai Institute of Technology, Lianyungang 222005, China (e-mail: lemonmiao@gmail.com).

A. Sowmya is with the School of Computer Science and Engineering, University of New South Wales, Sydney, NSW 2052, Australia (e-mail: sowmya@unsw.edu.au).

Z. Wei and B. Zheng are with the Department of Information Science and Engineering, Ocean University of China, Qingdao 266061, China (e-mail: weizhiqiangou@gmail.com; bingzh@ouc.edu.cn).

Digital Object Identifier 10.1109/JOE.2018.2886093

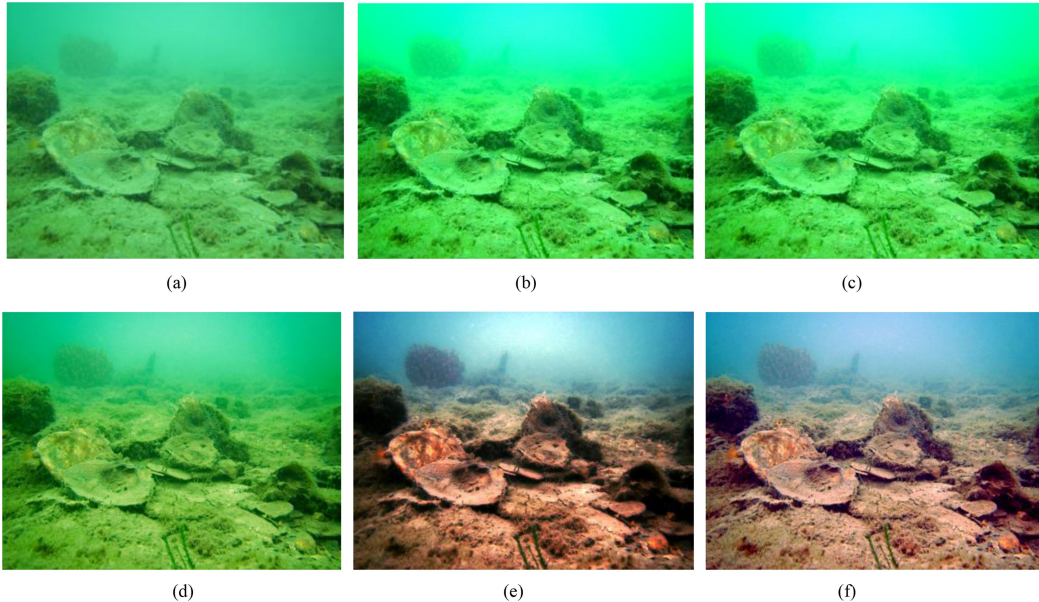


Fig. 1. Examples of the results produced by the DCP based underwater image restorations, from top to down, left to right are: (a) Original image. The restored results obtained by using: (b) [16], (c) [15], (d) [19], (e) [21], and (f) the proposed method.

map estimation by using the ambient light differential with a known background intensity value [20]. Li *et al.* [21] leveraged the quad-tree subdivision and graph-based segmentation to obtain a global background intensity and estimated the medium transmission map by the minimum information loss principle. Recently, nonuniform background lighting had been considered by several underwater dehazing methods [22], [23]. Emberton *et al.* [22] proposed a hierarchical rank-based method, where a set of features was used to obtain the most haze-opaque area. Ancuti *et al.* [23] introduced a local backscattering estimation method, in which the local maxima of the dark channel were selected as the background intensity.

The results of some of these methods on offshore underwater images are shown in Fig. 1. It can be seen that assuming a global value or assigning the maximum of the dark channel [14]–[21] as the background intensity in the DCP based restorations causes oversaturation and performs poorly on the restoration of clarity. Furthermore, transmission map estimation may be imprecise due to nonadaptive fixed-range transformation [16] when the original image has values that are physically impossible. In water medium, lighting attenuation in a wavelength-dependent manner causes different water colors [24], [25]. As the effect also depends on object distance, the degradations in underwater images show local characteristics and cannot be corrected by a global operation. It has been found that satisfactory results can be obtained by using appropriate enhancement methods for various underwater tasks and environments [26]. Therefore, restorations without considering the optical properties of different ocean areas cause unsatisfactory results in changing underwater environments.

In contrast, this paper proposes a novel method for underwater image restoration with a reflection-illumination decomposition based transmission map and local background lighting estimation. Based on the underwater imaging model and the

optical characteristics priors, a specific offshore underwater restoration technique is designed to handle the blurriness and the loss of Chroma. It differs from image enhancement methods such as that of Fu *et al.* [8]. Distinct from the methods which estimate the background lighting as a single value [14]–[21], background lighting maps are derived to obtain clearly restored edge details. A simpler computation step is performed compared to the Peng and Cosman [19], Li *et al.* [21], and Emberton *et al.* [22], and leads to a better restoration result. The specific contributions are as follows.

- 1) It introduces an underwater image restoration model by applying Retinex-decompositon on the dark channel and estimates the transmission map directly, which is a novel solution compared to the approaches in which a single approximate backscattering value is used as the denominator.
- 2) It summarizes the optical properties of the offshore water body and applies them as priors to yield a more effective restoration method for offshore areas.
- 3) It uses a local backscattering light estimation to get better clarity restoration. These innovations enable a significant and efficient improvement over other DCP based restoration methods for offshore underwater images on objective and subjective inspection.

The rest of this paper is organized as follows. The underwater imaging model and an analysis of the DCP based underwater image restoration are presented in Section II. In Section III, the framework of the proposed reflection decomposition based underwater image restoration model is described. Some optical properties of offshore areas are discussed, and details of the proposed offshore underwater restoration method are expressed in Section IV. Comparative experiments are presented in Section V. Finally, Section VI provides concluding remarks.

## II. RELATED WORK

Underwater restoration is an inverse process of the attenuation that occurs when light passes through water. In this section, the underwater imaging model and the restoration process based on the DCP are described. The estimation of backscattering light is a key step in DCP based underwater image restoration. While the majority of approaches make use of the maximum of the dark channel as the estimated background lighting, intensities are not uniformly distributed on the underwater image plane in practice.

### A. Jaffe-McGlamery Model

According to the Jaffe-McGlamery underwater imaging model [27], the total radiance of an image that reaches an observer is due to three additive components: direct component  $E_d$ , forward scattering component  $E_f$ , and backscattering component  $E_b$ .

$E_d$  represents the attenuated version of reflected light, and is expressed as follows:

$$E_d = J_c(x)e^{-p_\lambda d(x)} \quad (1)$$

where  $J_c(x)$  is the radiance of the object at point  $x$ ,  $c$  is the color channel in RGB space,  $c = \{R, G, B\}$ ,  $d(x)$  is the distance between the observer and the object, and  $p_\lambda$  is the attenuation coefficient. In underwater environments,  $p_\lambda$  is the sum of the absorption coefficient  $a_\lambda$  and the scattering coefficient  $b_\lambda$ , where both are wavelength  $\lambda$  dependent

$$p_\lambda = a_\lambda + b_\lambda. \quad (2)$$

The exponential term  $e^{-p_\lambda d(x)}$  is also known as the transmission map  $t_c(x)$  through the water medium

$$t_c(x) = e^{-p_\lambda d(x)}. \quad (3)$$

For offshore water (depth <20 m),  $E_b$  can be expressed as follows [22]:

$$E_b(x) = B_\infty^c(x)(1 - e^{-p_\lambda d(x)}) \quad (4)$$

where  $B_\infty^c(x)$  is known as the backscattering light of  $c = \{R, G, B\}$  channel [22] or the background light at pixel  $x$ . In general, forward scattering is associated with a small fraction of the overall image degradation, and the simplified underwater optical imaging model employed in most existing restoration techniques becomes

$$I_c(x) = J_c(x)t_c(x) + (1 - t_c(x))B_\infty^c(x). \quad (5)$$

By inserting underwater raw image  $I_c(x)$ ,  $B_\infty^c(x)$ , and  $t_c(x)$  into (5), the restored underwater image  $J_c(x)$  can be obtained from

$$J_c(x) = \frac{I_c(x) - B_\infty^c(x)}{t_c(x)} + B_\infty^c(x). \quad (6)$$

### B. Underwater Image Restoration Based on the DCP

Based on the DCP [14], the dark channel  $L_{DC}$  of an underwater color image  $I_c(x)$  is computed by the minimization in local

patches  $\Omega(x)$  over  $R, G$ , and  $B$  channels

$$L_{DC}(x) = \min_{y \in \Omega(x)} \left( \min_{c \in \{R, G, B\}} I_c(y) \right). \quad (7)$$

To estimate the transmission map  $t_c(x)$ , usually the state-of-the-art methods compute the maximum of  $L_{DC}$ , and select the corresponding pixel values in the input image as the global background light [12], [14]–[17]. Dividing both sides of (5) by  $B_\infty^c(x)$  and applying the minimum operators, gives

$$\begin{aligned} \min_{y \in \Omega(x)} \left( \min_{c \in \{R, G, B\}} \frac{I_c(y)}{B_\infty^c(y)} \right) &= \min_{y \in \Omega(x)} \left( \min_{c \in \{R, G, B\}} \frac{J_c(y)}{B_\infty^c(y)} t_c(y) \right) \\ &+ 1 - \min_{y \in \Omega(x)} \left( \min_{c \in \{R, G, B\}} t_c(y) \right). \end{aligned} \quad (8)$$

Applying DCP [14] to the original image  $J_c(x)$ , we have

$$\min_{y \in \Omega(x)} \left( \min_{c \in \{R, G, B\}} J_c(y) \right) = 0. \quad (9)$$

Based on (8) and (9), the DCP based methods estimate the transmission map as follows [14]:

$$\tilde{t}_c(x) = 1 - \min_{y \in \Omega(x)} \left( \min_{c \in \{R, G, B\}} \frac{I_c(y)}{\tilde{B}_\infty^c(y)} \right). \quad (10)$$

Where  $\tilde{t}_c(x)$  and  $\tilde{B}_\infty^c(x)$  are the estimated transmission map and background light, respectively. Underwater image restoration or dehazing methods based on DCP construct the dark channel image in various ways [14]–[21]. Carlevaris-Bianco *et al.* [16] computed the dark channel image by the difference between the maximum in the red channel and other channels (green and blue), and calculated the estimated transmission map by adjusting the difference to one. Galdran *et al.* [15] also used the reciprocal of a single background lighting to obtain the transmission map on the red channel, and computed the transmission map on the other two channels with the prior of the attenuated coefficients. Peng *et al.* [18] proposed a transmission map based on max filtering on the image blurriness. Li *et al.* [21] estimated the medium transmission map by combining the minimum information loss principle with (10), and obtained a single value for the background light.

Most methods take the brightest pixel in the dark channel image as the estimated background light. However, a single  $\tilde{B}_\infty^c$  value over the entire image fails to explain the real interaction of light rays and the particles in the water medium [28]. On the one hand, since three-dimensional space is sliced into planes to compute the irradiance of each illuminated slab in different directions and distances, the background light can be viewed as a superposition of many point-sources of light in space if the thickness of the backscattering volume unit can be ignored compared with the distance between lighting source and camera, which will produce gradations in the image intensity. On the other hand, environmental light also suffers from scattering by floating particles. To show the real distribution of underwater lighting intensities, the irradiance of the different areas on a flat board (checkerboard 110 cm × 182 cm with 10 × 7 patches) placed in a tank under daylighting were measured, as

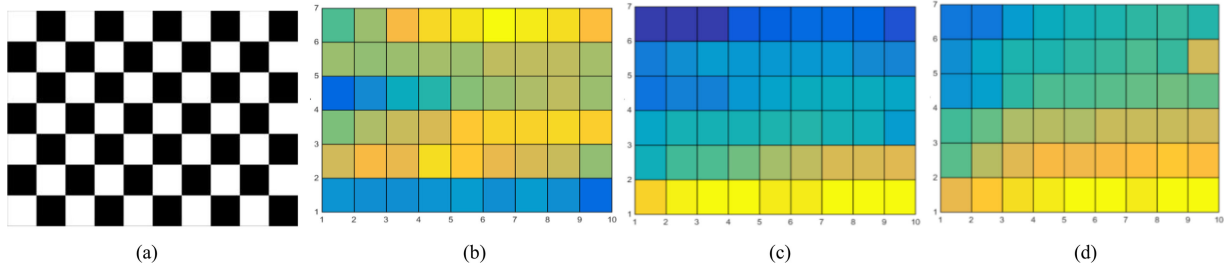


Fig. 2. Irradiance distributions of the target board at 60 cm distance from the camera in a tank under daylighting. (a) Target. (b) Clear water. (c) Medium turbidity. (d) Turbidity.

shown in Fig. 2(a). The tank is 2 m long, 1.2 m wide, and 1 m high. Every test was repeated five times under the conditions of clear, medium muddy, and turbid water, and the average of each corresponding image block was computed. The fitted irradiance distributions of the target board are shown in Fig. 2(b)–(d). It can be observed that the intensities are not distributed uniformly on an image plane. When the dark channel image is used to compute the transmission map, under- or oversaturation occur when the brightest value of the image is used as the denominator in (10). Artefacts in the background regions are caused by the low transmission values in these parts of the scene [29].

### III. UNDERWATER IMAGE RESTORATION BASED ON REFLECTION DECOMPOSITION

Inspired by the light reflection model, we propose a DCP based underwater image restoration algorithm, which includes color correction. A novel dark channel decomposition method is utilized to estimate the transmission map directly and a locally Gaussian background lighting estimation is applied. The framework of the proposed method is shown in Fig. 3.

#### A. Transmission Map Estimation

By applying the minimum operators to (5) and with (7) and (9), the dark channel of an underwater color image  $I_c(x)$  is

$$L_{DC}(x) = \tilde{B}_\infty(x)(1 - \tilde{t}_c(x)). \quad (11)$$

where  $\tilde{B}_\infty(x)$  is the minimization of estimated  $\tilde{B}_\infty^c(x)$  on three channels,  $\tilde{B}_\infty(x) = \min_{y \in \Omega(x)}(\min_{c \in \{R, G, B\}} \tilde{B}_\infty^c(y))$ .  $\tilde{t}(x)$  is the minimization of  $\tilde{t}_c(x)$  on three channels within the range  $[0, 1]$ ,  $\tilde{t}(x) = \min_{y \in \Omega(x)}(\min_{c \in \{R, G, B\}} \tilde{t}_c(y))$ . Given (11),  $L_{DC}$  can be described as follows [30]:

$$L_{DC} = \tilde{B}_\infty(x) \cdot \tilde{T}(x) \quad (12)$$

where  $\tilde{T}(x) = 1 - \tilde{t}(x)$ . As described in the underwater imaging model [27],  $\tilde{B}_\infty(x)$  is irrelevant to the object, while  $\tilde{t}(x)$  describes the proportion of the object irradiance arriving at the camera without absorption and scattering. According to the Retinex theory [31]–[33], a grayscale image can be described as a product of the illumination and the reflectance. The proposed novel solution decomposes the  $\tilde{B}_\infty(x)$  and the transmission map related  $\tilde{T}(x)$  from  $L_{DC}$ . Then the estimated transmission map

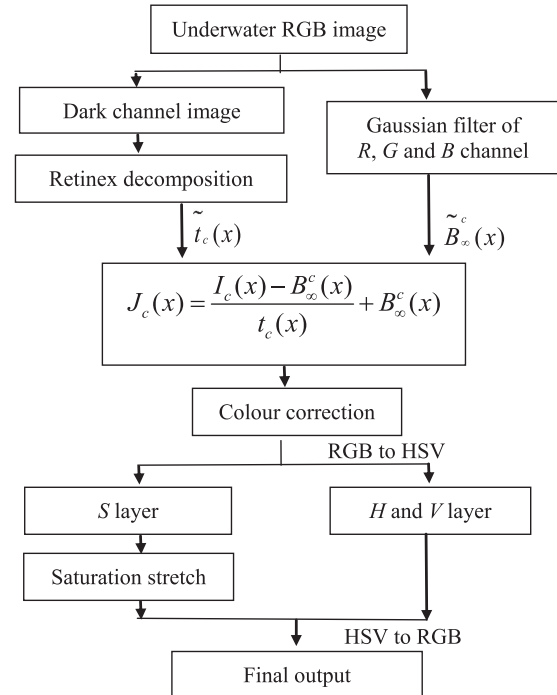


Fig. 3. Framework of the proposed underwater image restoration method.

$\tilde{t}(x)$  can be computed by

$$\tilde{t}(x) = 1 - \tilde{T}(x). \quad (13)$$

Many algorithms have been proposed to address the illumination-reflectance estimation by logarithmic transformation including classical single scale Retinex [34], multiscale Retinex [35], and multiscale Retinex with color restoration (MSRCR) [36]. Recursive matrix calculation was adopted by McCann [37]. Kimmel *et al.* [38] proposed the variational frame of Retinex, and the L2-fidelity prior was used by Ng and Wang [39].

#### B. Backscattering Light Estimation

According to Schechner and Karpel [4], backscattering is the prime reason for underwater image contrast degradation. Unlike direct attenuation and forward scattering components, background light does not originate from the object. Instead, it is caused by the scattering of the ambient light by suspended

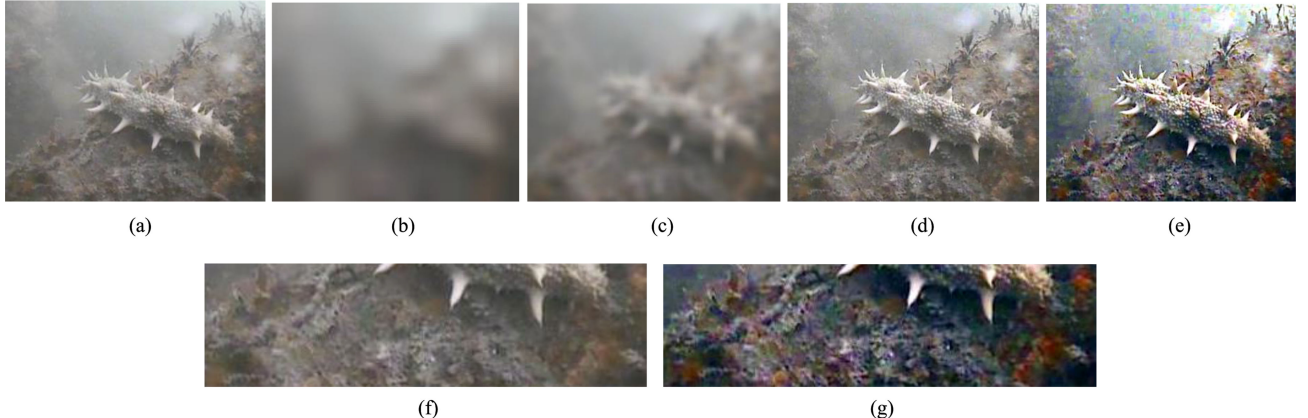


Fig. 4. Backscattering light estimations. (a) Original image. (b) Backscattering light obtained using Ancuti *et al.* [23]. (c) Backscattering light of the proposed method. (d) Final result obtained using Ancuti *et al.* [23]. (e) Result of the proposed method. (f) Local detail of the result produced by Ancuti *et al.* [23]. (g) Local detail of the result produced by the proposed method.

particles in water from a large distribution of angles. Research has shown that light-rays traveling in an underwater environment encounter beam–particle interaction with different random times. Therefore, a local backscattering estimation is better adapted to underwater environments [22], [23].

Given an underwater color image  $I_c(x)$  with three channel intensity values between 0 and 1, a local patch in the image has a uniform distance to the camera. The backscattering light is estimated using Gaussian lowpass filtering of the observed image, which is inspired by the initial illumination estimation in the MSRCR [36] method

$$\tilde{B}_\infty^c(x) = G_\Omega(x) \otimes (I_c(x)) \quad (14)$$

where  $G_\Omega(x)$  is the Gaussian function,  $\otimes$  is the convolution operation, and  $\Omega(x)$  is a local window around pixel  $x$ . An example of the backscattering light estimation is shown in Fig. 4. It can be seen from Fig. 4(f) and (g) that, the proposed local backscattering light estimator provides a more refined detail restoration than the local backscattering light estimation proposed by Ancuti *et al.* [23].

### C. Color Correction

The next step is to perform the color correction on the descattered image to compensate for possible color casts. A statistical colorless slant correction method is adopted. For a restored underwater image  $J_c(x)$ , the maximum and minimum of  $R$ ,  $G$  and  $B$  channels are defined as follows:

$$J_{\max}^c = J_{\text{mean}}^c + \mu J_{\text{var}}^c \quad (15)$$

$$J_{\min}^c = J_{\text{mean}}^c - \mu J_{\text{var}}^c \quad (16)$$

where  $J_{\text{mean}}^c$  and  $J_{\text{var}}^c$  are the mean value and square error in channel  $c$ , respectively.  $\mu$  is a parameter to control the image dynamic, and the empirical range of  $\mu$  is between 2 and 5. The color corrected image  $J_{\text{CR}}^c$  [8] is

$$J_{\text{CR}}^c = \frac{J^c - J_{\min}^c}{J_{\max}^c - J_{\min}^c}. \quad (17)$$

After the color casting is compensated, a contrast stretch on the saturation layer in Hue Saturation Value space is performed

since, in general, the restored images tend to be under- or over-saturated.

## IV. OFFSHORE UNDERWATER IMAGE RESTORATION

The attenuation coefficient for the global ocean shows significant spatial and temporal variation as it depends on the concentration of organic and inorganic substances in the water column. This variation has implications for the underwater computer vision where the attenuation information is used for visibility enhancement and in color restoration algorithms. A visibility enhancement algorithm whose parameters are derived from clear water would perform poorly when applied to images from an environment which is characterized by a strong light attenuation. For a specific camera and distance, the attenuation coefficients of seawater have two options, for open water and coastal respectively [40]. As a special case, the offshore areas have unique optical characteristics. The depth of offshore water is shallow, and concentrations of colored dissolved organic matter (cDOM) and total suspended matter (TSM) are higher than at far-shore because of the impact of terrigenous input and sediment resuspension [41]. Optical field measurement data have shown great differences between optical properties of the offshore and farshore areas [42], e.g., most offshore areas of China belong to case-II water, dominated by type-D and E. Type-D water appears closer to yellowish-green [43], [44], compositions of which are mainly the suspended-sediments tripton and cDom. Type-E water is turbid due to the influence of the terrestrial source input, the dominant component of which is tripton. Therefore, the absorption of tripton and cDom and the scattering caused by TSM are the main sources of degradation for offshore underwater images. TSM does not absorb light, and the scattering of visible light produces similar  $R$ ,  $G$  and  $B$  luminance, and makes the image appear covered by white veiling [45]. The following can be concluded from the offshore optical field measurement data [42].

- 1) The absorption coefficient of offshore water shows a trend of exponential decay, the scattering and attenuation coefficients decrease gradually with increasing wavelength.

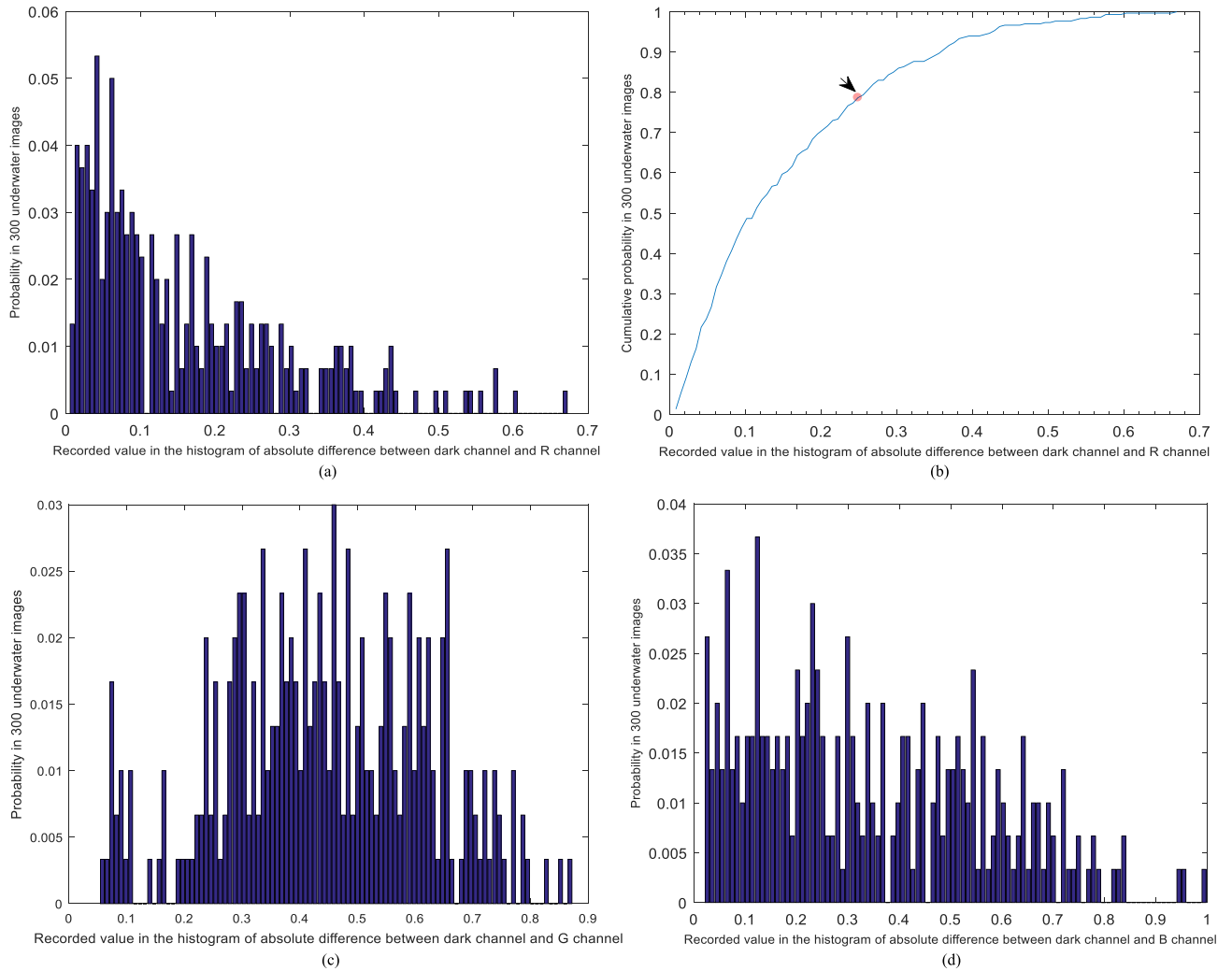


Fig. 5. Histograms of the absolute differences distributions between  $L_{DC}$  and  $R$ ,  $G$  and  $B$  channels in 300 underwater images. (a) Histogram of the record, where the value corresponds to 75% pixels in the histogram of absolute difference between  $L_{DC}$  and  $R$ . (b) Cumulative histogram distribution of (a). (c) Corresponding histogram between  $L_{DC}$  and  $G$ . (d) Corresponding histogram between  $L_{DC}$  and  $B$ .

- 2) The maxima of all coefficients occur in near shore, such as estuary, shoal, and bay areas.
- 3) The absorption coefficient of an offshore area water body has substantially higher average value than the scattering coefficient which has average value between  $10^{-2} - 10^{-1}$ , and the deviation of scattering coefficients is small.

The absorption of depigmented particles is a particularly dominant degradation factor in offshore areas, and generally contributes over 50% to the absorption coefficient. The cDOM absorption is the second part that contributes less than 35%. Therefore, the attenuation coefficient  $p_\lambda$  can be simplified with  $a_\lambda$ . For offshore areas, the decay of the absorption coefficient  $a_\lambda$  can be described as follows [43]:

$$a_\lambda = a_{\lambda_0} \exp[-S_x(\lambda - \lambda_0)] \quad (18)$$

where  $\lambda_0 = 440$  nm is the reference wavelength.  $S_x$  is the empirical value. It has been proved that  $S_x$  is  $0.0049 - 0.0175 \text{ nm}^{-1}$  within the light wavelength range of 380–600 nm,

by applying least-square fitting on offshore optical statistical data [43].

Based on the optical properties of water, long wavelength (red) light is attenuated in water more than short wavelength [22]. To obtain the most reasonable dark channel image for offshore image restoration, 300 daytime offshore (depth <20 m) underwater images were collected including sea farming, shallow sea creature investigation, and coastal underwater engineering images, some of which can be seen in the Section V. The normalized absolute difference between the dark channel image and the  $R$  channel of each image is calculated, and the position where the accumulated pixels are more than 75% of the total number of the image are recorded. The histogram of these records over all 300 offshore images is computed, as shown in Fig. 5(a). A window size of  $15 \times 15$  is used to compute the dark channel, and Fig. 5(b) is the corresponding cumulative distribution. Over 80% of the images in the data set have difference values of dark channel from  $R$  channel lower than 0.26, as pointed by the arrow in Fig. 5(b). The difference values of the  $G$  and  $B$  channels from the dark channel image are

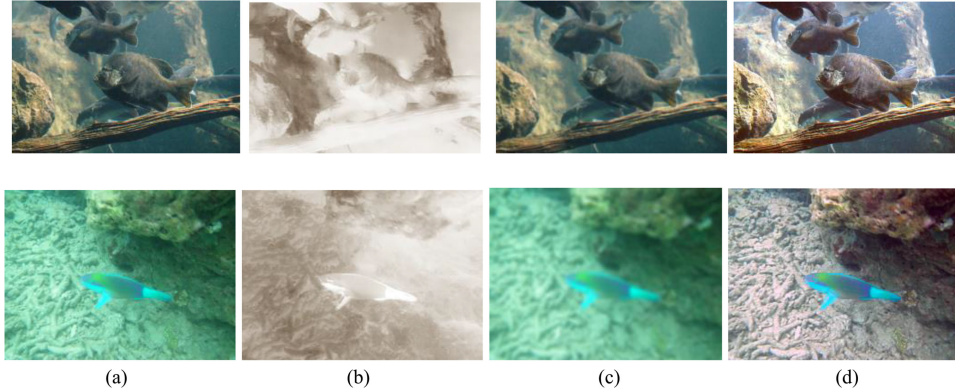


Fig. 6. Examples of the transmission map estimations and the final output images. (a) Original. (b) Transmission map. (c) Backscattering light. (d) Final output.

also computed, and the corresponding histograms are shown in Fig. 5(c) and (d). Again, most of the offshore images have dark channels approximate their  $R$  components, which means that the dark channel can be used to estimate the transmission map of  $R$  channel. Given this assumption, (12) can be rewritten as follows:

$$L_{DC} = \tilde{B}_\infty(x) \cdot \tilde{T}_R(x). \quad (19)$$

Here, the transmission map is estimated from  $L_{DC}$  by the linear-domain Retinex decomposition proposed by Fu *et al.* [46]. It can be seen as a posterior distribution via Bayes's theorem

$$p(\tilde{T}_R, \tilde{B}_\infty | L_{DC}) \propto p(L_{DC} | \tilde{T}_R, \tilde{B}_\infty) p(\tilde{B}_\infty) p(\tilde{T}_R) \quad (20)$$

where  $p(\tilde{T}_R, \tilde{B}_\infty | L_{DC})$  is the posterior distribution,  $p(L_{DC} | \tilde{T}_R, \tilde{B}_\infty)$  is the likelihood.  $p(\tilde{T}_R)$  and  $p(\tilde{B}_\infty)$  represents the prior probabilities on the estimated backscattering light  $\tilde{B}_\infty(x)$  and the estimated  $\tilde{T}_R(x)$ , respectively.

The estimation of  $\tilde{T}_R$  is accomplished by minimization of the objective function with the alternating direction method of multipliers (ADMM) [47]

$$\begin{aligned} E(\tilde{B}_\infty, \tilde{T}_R) &= \left\| \tilde{B}_\infty \cdot \tilde{T}_R - L_{DC} \right\|_2^2 + \eta \left\| \nabla \tilde{B}_\infty \right\|_2^2 \\ &\quad + \beta \left\| \nabla \tilde{T}_R \right\|_1 + \gamma \left\| \tilde{B}_\infty - \tilde{B}_0 \right\|_2^2 \\ \text{s.t. } L_{DC} &\leq \tilde{B}_\infty \end{aligned} \quad (21)$$

where  $\eta, \beta, \gamma$  are three positive parameters and  $\|\cdot\|$  denotes the  $p$ -norm operator. The empirical values of  $\eta, \beta, \gamma$  are set at 1000, 0.01, and 0.1, and the analysis about the value selection can be found in [46].  $\tilde{B}_0$  is the mean estimation of background light. Then, the estimated transmission map on red channel  $\tilde{t}_R$  can be obtained by (13). By applying (18) to (2), following can be obtained:

$$\frac{p_G}{p_R} \approx \frac{\alpha_G}{\alpha_R} = \frac{\exp[-S_x(\lambda_G - \lambda_0)]}{\exp[-S_x(\lambda_R - \lambda_0)]} \quad (22)$$

$$\frac{p_G}{p_R} \approx \frac{\alpha_B}{\alpha_R} = \frac{\exp[-S_x(\lambda_B - \lambda_0)]}{\exp[-S_x(\lambda_R - \lambda_0)]}. \quad (23)$$

---

**Algorithm 1:** Offshore Underwater Image Restoration Algorithm.

---

**Input:** Observed image  $I_c(x)$ , Gaussian filtering scale  $\Omega$  and the variance in backscattering light estimation, parameters in the adopted Retinex model.

For the variational linear domain probabilistic method adopted, parameters include  $\eta, \beta, \gamma$  in ADMM.

**Step 1:** Compute the dark channel image  $L_{DC}$  using (7).

**Step 2:** Estimate  $\tilde{T}_R(x)$  by using Retinex illumination reflection decomposition on (19) and obtain  $\tilde{t}_R(x)$  by (13).

**Step 3:** Compute  $\tilde{t}_G(x)$  and  $\tilde{t}_B(x)$  by (24) and (25).

**Step 4:** Estimate the backscattering light  $\tilde{B}_\infty^c(x)$  by (14) on three channels.

**Step 5:** Restore offshore underwater image by using (6).

**Step 6:** Output the final corrected image by applying (17) and saturation adjustment.

---

Then, estimate  $\tilde{t}_G(x)$  and  $\tilde{t}_B(x)$  as follows:

$$\tilde{t}_G(x) = e^{-p_G d(x)} = (e^{-p_R d(x)})^{\frac{p_G}{p_R}} = (\tilde{t}_R(x))^{\frac{p_G}{p_R}} \quad (24)$$

$$\tilde{t}_B(x) = e^{-p_B d(x)} = (e^{-p_R d(x)})^{\frac{p_B}{p_R}} = (\tilde{t}_R(x))^{\frac{p_B}{p_R}}. \quad (25)$$

After obtaining the estimated transmission map, a guided filter [47] is incorporated to refine it. Examples of the estimated transmission maps and the final restored results are shown in Fig. 6. It can be seen that using the illuminance and reflection decomposition generates a more visually pleasing result. Details of the offshore underwater image restoration algorithm are summarized in Algorithm 1.

In Section V, experimental results are presented to demonstrate the efficiency and effectiveness of the proposed method.

## V. TESTS AND QUALITY EVALUATION

The proposed approach was validated on offshore underwater images. The data include 300 RGB images collected from online underwater images associated with offshore investigation, sea farming or offshore eutrophic areas, size averaging from  $194 \times 259$  to  $3968 \times 2976$ . In the experiments, the block sizes



Fig. 7. Restoration comparisons. (a) Original image. The restored results obtained by using: (b) [16], (c) [15], (d) [19], (e) [21], and (f) the proposed method.

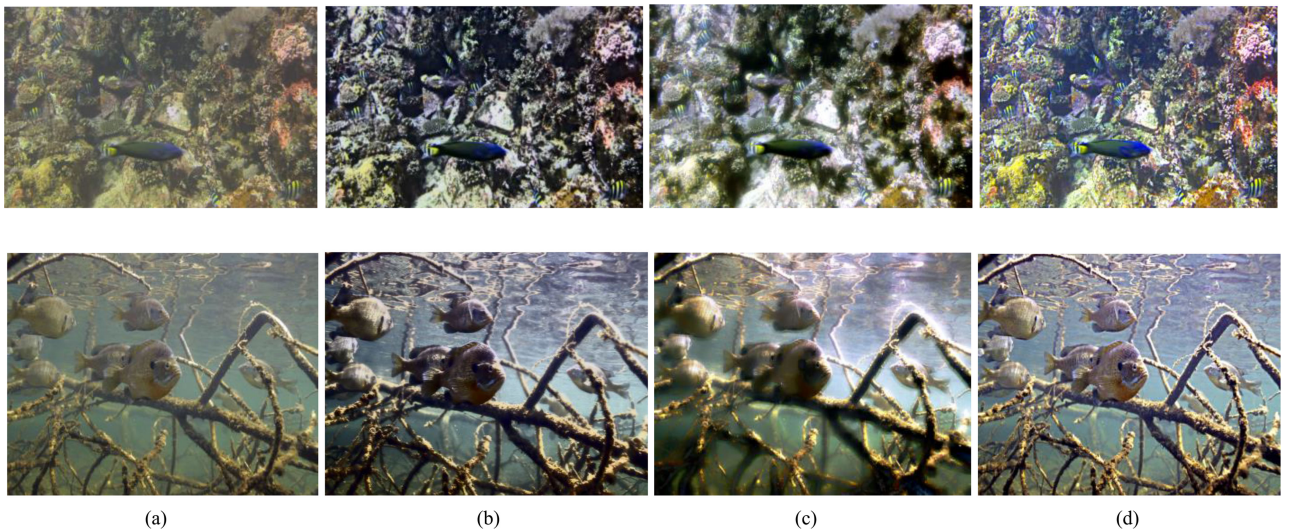


Fig. 8. Restoration comparisons. (a) Original image. The restored results obtained by using: (b) [8], (c) [21], and (d) the proposed method.

of the dark channel and Gaussian filter were  $15 \times 15$ . The empirical parameters  $\eta, \beta, \gamma$  were set to 1000, 0.01, and 0.1 [46].

#### A. Subjective Inspection

The proposed method was compared with other relevant state-of-the-art methods including those proposed by Carlevaris-Bianco *et al.* [16], Galdran *et al.* [15], Fu *et al.* [8], Peng and Cosman [19], and Li *et al.* [21]. Some of these experimental

results are shown in Figs. 7 and 8. It can be seen from the edges in the results that the proposed method achieved better deblurring and color restoration effect comparable with the outputs of Carlevaris-Bianco *et al.* [16], Galdran *et al.* [15], Fu *et al.* [8], Peng and Cosman [19], and Li *et al.* [21]. Although the algorithm proposed by Li *et al.* [21], and the method applying Retinex decomposition on the illuminance channel proposed by Fu *et al.* [8] recover color visually, they lose clarity of detail and tend to emphasize the dark areas, as shown in Fig. 8.

TABLE I  
QUANTITATIVE MEASUREMENT RESULTS

| Image shown in Fig. 7                | Contrast of brightness | Saturation average | Chroma variance | UCIQE         |
|--------------------------------------|------------------------|--------------------|-----------------|---------------|
| Original image                       | 0.6314                 | 0.8118             | 0.2534          | 0.5010        |
|                                      | 0.8275                 | 0.7542             | 0.2923          | 0.5582        |
|                                      | 0.6941                 | 0.7864             | 0.2761          | 0.5223        |
|                                      | 0.4902                 | 0.7705             | 0.1684          | 0.4119        |
| Carlevaris-Bianco <i>et al.</i> [16] | 0.8353                 | 0.8352             | 0.2820          | 0.5764        |
|                                      | <b>0.9373</b>          | 0.7582             | <b>0.3911</b>   | <b>0.6356</b> |
|                                      | 0.8706                 | 0.8072             | 0.3157          | 0.5946        |
|                                      | 0.6196                 | 0.8010             | 0.1916          | 0.4661        |
| Galdran <i>et al.</i> [15]           | 0.7725                 | 0.8357             | 0.3230          | 0.5785        |
|                                      | 0.9098                 | 0.7729             | 0.2992          | 0.5889        |
|                                      | 0.7255                 | 0.8190             | 0.2735          | 0.5381        |
|                                      | 0.7333                 | 0.8547             | 0.1975          | 0.5139        |
| Peng <i>et al.</i> [19]              | <b>0.9843</b>          | <b>0.8818</b>      | <b>0.4529</b>   | <b>0.7093</b> |
|                                      | 0.9294                 | <b>0.8338</b>      | 0.3062          | <b>0.6132</b> |
|                                      | 0.9216                 | <b>0.8612</b>      | <b>0.3315</b>   | 0.6300        |
|                                      | 0.6941                 | 0.7414             | 0.2268          | 0.4877        |
| Li <i>et al.</i> [21]                | 0.0941                 | 0.5877             | 0.0652          | 0.2062        |
|                                      | 0.1216                 | 0.5845             | 0.1541          | 0.2560        |
|                                      | 0.1216                 | 0.5849             | 0.1600          | 0.2589        |
|                                      | 0.1216                 | 0.5848             | 0.1372          | 0.2482        |
| Proposed method                      | 0.8745                 | 0.8132             | 0.3441          | 0.6106        |
|                                      | 0.8235                 | 0.8096             | 0.3456          | 0.5963        |
|                                      | <b>0.9647</b>          | 0.8030             | 0.2992          | <b>0.6117</b> |
|                                      | <b>0.9294</b>          | 0.8204             | <b>0.3231</b>   | <b>0.6177</b> |

TABLE II  
QUANTITATIVE MEASUREMENT RESULTS

| Image shown in Fig. 8 | Contrast of brightness | Saturation average | Chroma variance | UCIQE         |
|-----------------------|------------------------|--------------------|-----------------|---------------|
| Original image        | 0.5216                 | 0.8476             | 0.2417          | 0.4746        |
|                       | 0.6824                 | 0.8452             | 0.2475          | 0.5209        |
| Fu <i>et al.</i> [8]  | <b>0.8588</b>          | <b>0.8796</b>      | 0.2434          | 0.5762        |
|                       | 0.8627                 | <b>0.8512</b>      | 0.2704          | 0.5826        |
| Li <i>et al.</i> [21] | 0.0941                 | 0.5807             | 0.0891          | 0.2171        |
|                       | 0.0941                 | 0.5846             | 0.1630          | 0.2527        |
| Proposed method       | 0.8275                 | 0.8247             | <b>0.3524</b>   | <b>0.6045</b> |
|                       | <b>0.9961</b>          | 0.8022             | <b>0.3217</b>   | <b>0.6306</b> |

### B. Objective Measure

Since underwater color image quality evaluation (UCIQE) [49] is a well-accepted metric to qualify the comprehensive performance of an underwater image on contrast, saturation, and chroma [12], [18]–[21], [23], the results were compared on these metrics and the UCIQE value, as listed in Tables I and II, the highest metric values are shown in bold. As the tables show, the proposed approach achieved higher contrast gain, chroma variance, and the UCIQE values than the cited algorithms on most of the images shown in Figs. 7 and 8. For the first and second images in Fig. 7(b) and (d), the output images have areas that are too dark, which induce abnormally higher global contrasts and saturation averages. Accordingly, their UCIQE values rise as listed in Table I. It can be seen from Table II, that Fu *et al.* [8] and Li *et al.* [21] improved the color saturation but produced lower chroma variance, which indicate the blurring of detail in the output images, as shown in Fig. 8. For the

yellow-greenish, veil-covered offshore underwater images, the proposed method produced better clarity of detail, more uniform contrast and balanced saturation, and obtained more satisfactory colorfulness restorations.

To compare the applicability of the proposed method on offshore underwater images with other methods, the histograms of the metric values of the restored images improved by the proposed method over those of the 300 raw images are presented in Fig. 9. By applying the proposed method, contrast of 273 images was improved, of which 80% contrast values increased by at least 20%; the saturation average of 173 images was improved; for 291 images, the chroma variance was improved. In 296 images, the final UCIQE values were improved significantly, most of which increased by 20%–100%. Since some of the original images include dark areas, the saturations of the images restored by the proposed model decreased, as shown in Fig. 9(a). For comparative analysis, the histogram of the UCIQE

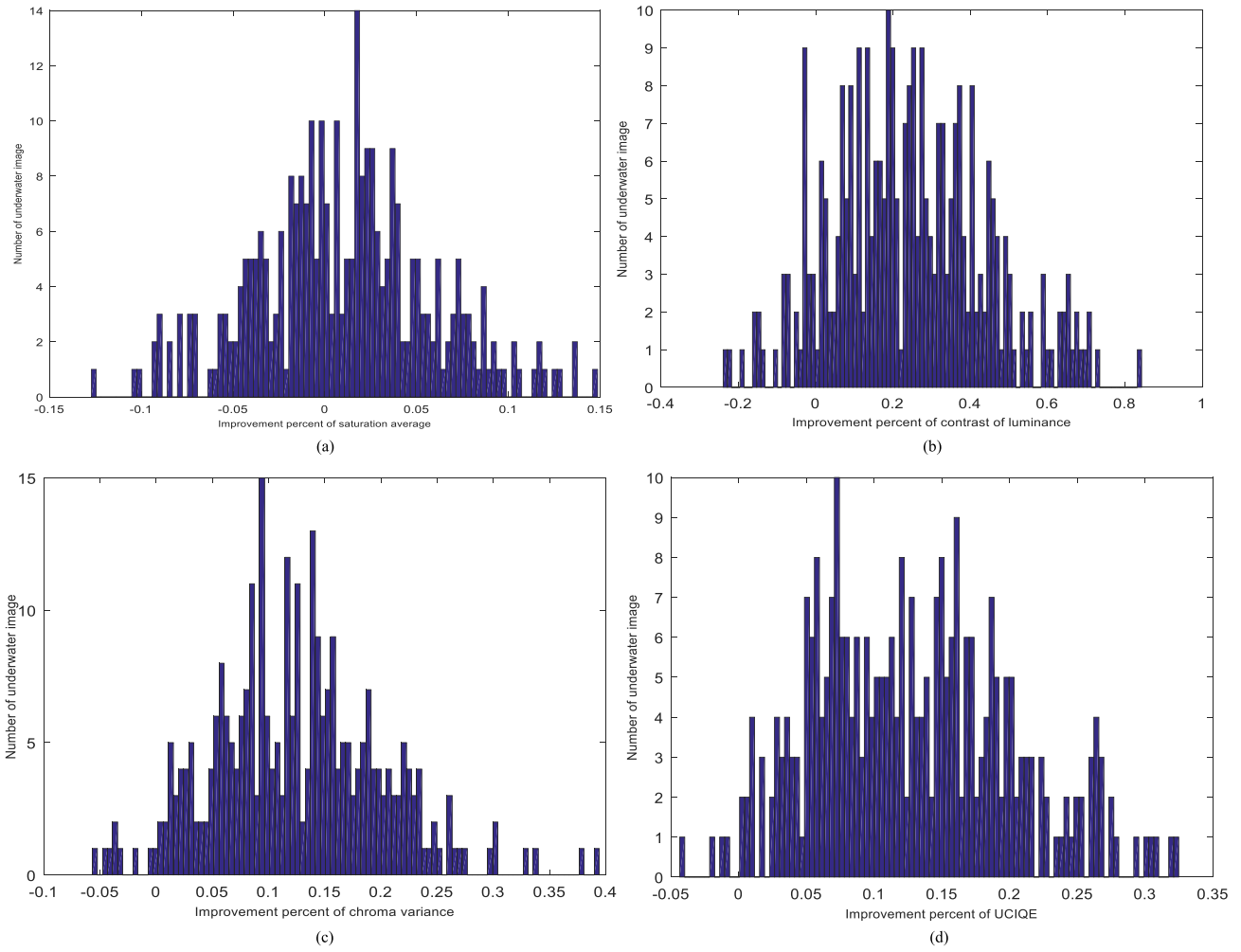


Fig. 9. Improvement histograms of underwater image quality metrics on 300 underwater images. (a) Saturation average. (b) Contrast of luminance. (c) Chroma variance. (d) UCIQE.

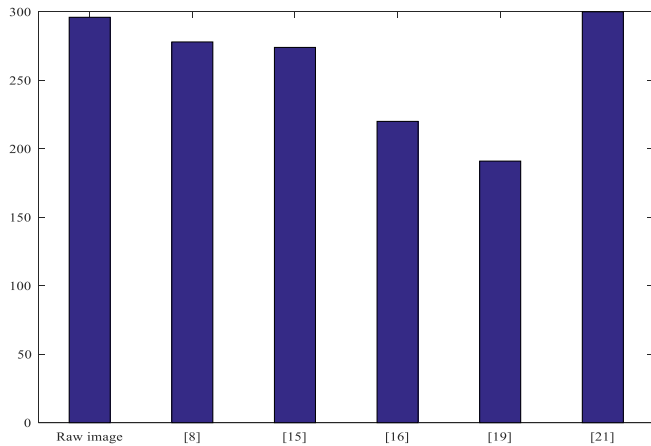


Fig. 10. Histogram of UCIQE values of the proposed approach higher than that of raw images and the state-of-the-art methods.

values of the proposed approach higher than the state-of-the-art methods on 300 offshore underwater images is shown in Fig. 10. The statistical results in Fig. 10 show that the proposed approach provide better improvements than other methods, with 278, 275,

220, and 191 images with higher improvements than Fu *et al.* [8], Galdran *et al.* [15], Carlevaris *et al.* [16], and Peng and Cosman [19], respectively, and 300 images with higher improvements than Li *et al.* [21].

### C. Restoration Accuracy

Imatest [50] is a professional software used in qualifying camera imaging by comparing the difference between real images of the charts and test images. To further verify the restoration capability of the proposed method objectively, comparisons with real charts are discussed by presenting the qualities of the restored Imatest 4.3 SFR chart and ColorChecker images taken in a tank. The tank is 2.53 m long, 1.02 m wide, and 1.03 m high. The Imatest SFR and ColorChecker 24 X-Rite Chart ( $21.59 \times 27.94$  cm) targets [50] are shown in Fig. 11. The images ( $960 \times 576$ ) were taken with OTI-UWC-325/ P/ E color camera in 94.5 cm transparency water [51] and under daylighting.

The relative contrast at a given spatial frequency (output contrast/input contrast) is called the modulation transfer function (MTF). It is a metric to measure image sharpness. Experience has shown that the best indicators of image sharpness are the

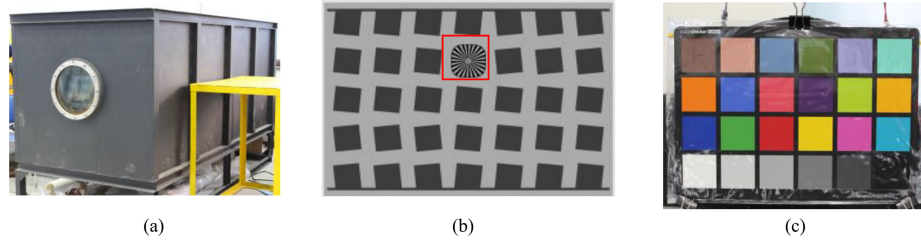


Fig. 11. Tank and targets. (a) Tank. (b) SFR chart. (c) ColorChecker chart.

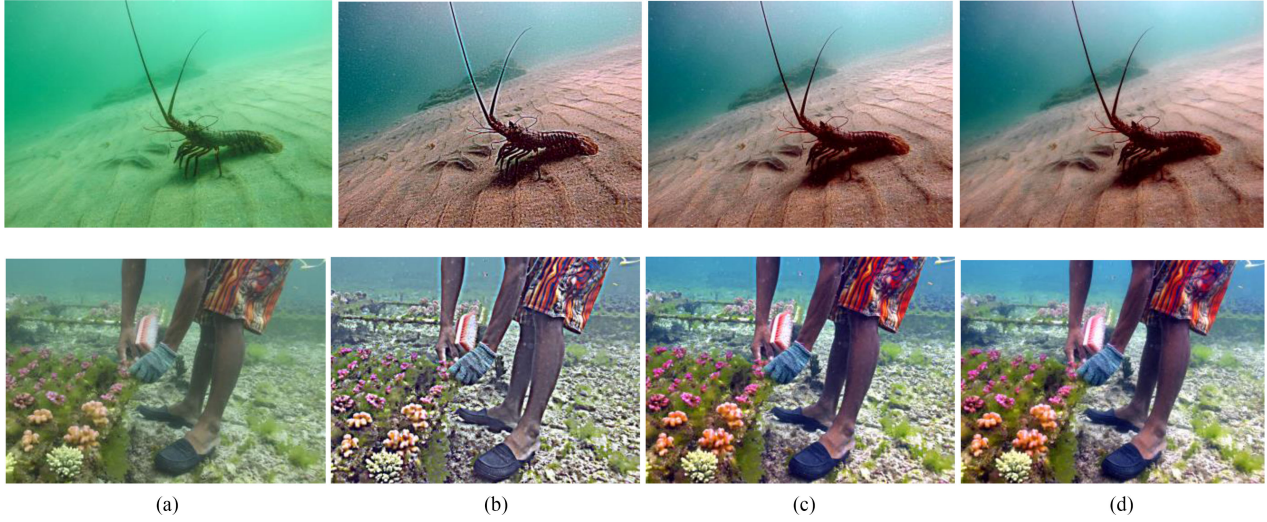


Fig. 12. Restoration comparisons with different Retinex models. (a) Original image. (b) McCann [37]. (c) Variational model in linear domain [46]. (d) MSRCR [36].

TABLE III  
IMATEST 4.3 SFR ANALYSIS

| SFR/analysis                         | MTF50 /(LW/PH ) |
|--------------------------------------|-----------------|
| Original image                       | 16.37           |
| Carlevaris-Bianco <i>et al.</i> [16] | 13.45           |
| Galdran <i>et al.</i> [15]           | 17.62           |
| Fu <i>et al.</i> [8]                 | 10.39           |
| Peng <i>et al.</i> [19]              | 17.08           |
| Li <i>et al.</i> [21]                | 20.51           |
| Proposed method                      | <b>22.56</b>    |

spatial frequencies where the MTF is 50% of its low frequency value (MTF50), and the unit line widths/picture height (LW/PH) is more convenient for the digital sensors. The data output for the central red box [see Fig. 11 (b)] from the Imatest 4.3 is listed in Table III. The data show that the proposed method achieves the best clarity. The color errors in the CIELAB space illustrate the capability of color restoration of the proposed algorithm. CIELAB color space was designed to be perceptually uniform,  $L$  is luminance,  $a$  and  $b$  are green-magenta, blue-yellow increment, respectively. The perceived color differences between the restored image and the real chart can be approximated by the Euclidean distance between them. In the CIELAB color space,

TABLE IV  
IMATEST 4.3 COLORCHECKER ANALYSIS

| Colour/analysis                      | $\Delta E_{ab}^*$ | $\Delta C_{ab}^*$ |
|--------------------------------------|-------------------|-------------------|
| Original image                       | 58.6              | 46.7              |
| Carlevaris-Bianco <i>et al.</i> [16] | 63.5              | 47.0              |
| Galdran <i>et al.</i> [15]           | 59.2              | 43.5              |
| Fu <i>et al.</i> [8]                 | 30.5              | 24.2              |
| Peng <i>et al.</i> [19]              | 52.7              | 48.9              |
| Li <i>et al.</i> [21]                | 32.1              | 29.5              |
| Proposed method                      | <b>29.4</b>       | <b>24.0</b>       |

$\Delta E_{ab}^*$  (which includes luminance  $L$ ) and  $\Delta C_{ab}^*$  (color only; omitting  $L$ ) listed in Table IV are computed by

$$\Delta E_{ab}^* = ((L_2 - L_1)^2 + (a_2 - a_1)^2 + (b_2 - b_1)^2)^{1/2} \quad (26)$$

$$\Delta C_{ab}^* = ((a_2 - a_1)^2 + (b_2 - b_1)^2)^{1/2}. \quad (27)$$

$\Delta C_{ab}^*$  or  $\Delta E_{ab}^*$  of around 1 corresponds roughly to a just noticeable difference between colors. It can be concluded from Tables III and IV that the proposed approach achieved the best performance on image sharpness and color restorations.

## D. Related Discussion

Next, the restoration results are compared to demonstrate the effects of the transmission map estimates when different Retinex models are applied, as shown in Fig. 12. In Fig. 12(b), sharper edges of the object are achieved by applying the Retinex model of McCann [37]. It produced relatively smooth results with MSRCR [36] and weak clarity restorations on farther objects in the images, as shown in Fig. 12(c). More satisfactory colorfulness restorations and better clarity of detail were exhibited in the results when the linear variational Retinex model was applied to the transmission map estimates. As for the scale of the Gaussian filter in the backscattering light estimation, edges would be over smoothed with an increased filter scale  $\Omega$ , which is similar to most Gaussian applications.

Finally, the computational time of the proposed method is tested. The test computer features 2.8 GHz frequency Intel i7 double-core CPU and 4 GB of RAM using Matlab 2016a. It takes about 1.03 s with an image size of  $541 \times 398$  when applying variational linear domain decomposition, and only about 0.60 s with the same image but using MSRCR [36] when estimating the transmission map. While the restoration process needs 31.48 and 1.20 s by Peng and Cosman [19] and Li *et al.* [21], respectively, the proposed method is less time consuming with better output.

## VI. CONCLUSION

The proposed approach aims to apply existing ocean optical measurements as a prior and restore offshore underwater images characterized by a heavy concentration of tripton and cDom. It introduces an underwater restoration model based on lighting-reflection decomposition, and applies optical priors of offshore water to obtain the transmission map. It refines the backscattering lighting estimation by a local estimator on  $R$ ,  $G$  and  $B$  channels. The results produced by the new method show good performance and wide applicability in comparison to the state-of-the-art across the tested offshore underwater images. More than 90% UCIQE values were improved significantly in the 300 offshore underwater images. It can be inferred that with the optical priors of different water areas, such as deep seawater, the proposed approach can achieve desirable results on most underwater images.

## REFERENCES

- [1] R. Gibson, R. Atkinson, and J. Gordon, "A review of underwater stereo image measurement for marine biology and ecology applications," *Oceanogr. Mar. Bio., Annu. Rev.*, vol. 47, pp. 257–292, 2016.
- [2] D. He and G. Seet, "Divergent-beam lidar imaging in turbid water," *Opt. Lasers Eng.*, vol. 41, no. 1, pp. 217–231, 2004.
- [3] E. Nascimento, M. Campos, and W. Barros, "Stereo based structure recovery of underwater scenes from automatically restored images," in *Proc. Conf. Graph., Patterns Images (SIBGRAPI)*, 2009, pp. 330–337.
- [4] Y. Y. Schechner and N. Karpel, "Recovery of underwater visibility and structure by polarization analysis," *IEEE J. Ocean. Eng.*, vol. 30, no. 3, pp. 570–587, Jul. 2005.
- [5] R. T. Tan, "Visibility in bad weather from a single image," in *Proc. IEEE Conf. Comput. Vis. Pattern Recognit.*, 2008, pp. 1–8.
- [6] K. Iqbal, R. Abdul Salam, A. Osman, and A. Zawawi Talib, "Underwater image enhancement using an integrated colour model," *Int. J. Comput. Sci.*, vol. 34, no. 2, pp. 529–534, 2007.
- [7] K. Iqbal, M. Odetayo, A. James, and R. Abdul Salam, "Enhancing the low quality images using unsupervised colour correction method," in *Proc. IEEE Int. Conf. Syst., Man Cybern.*, 2010, vol. 25, no. 1, pp. 1709–1709.
- [8] X. Fu, P. Zhuang, Y. Huang, Y. Liao, X.-P. Zhang, X. Ding, "A retinex-based enhancing approach for single underwater image," in *Proc. IEEE Int. Conf. Image Process.*, 2015, pp. 4572–4576.
- [9] J. Y. Chiang and Y. C. Chen, "Underwater image enhancement by wavelength compensation and dehazing," *IEEE Trans. Image Process.*, vol. 21, no. 4, pp. 1756–1769, Apr. 2012.
- [10] C. Ancuti, C. O. Ancuti, T. Haber, and P. Bekaert, "Enhancing underwater images and videos by fusion," in *Proc. IEEE Conf. Comput. Vis. Pattern Recognit.*, 2012, vol. 6428, no. 10, pp. 81–88.
- [11] J. P. Tarel and N. Hautière, "Fast visibility restoration from a single color or gray level image," in *Proc. IEEE Int. Conf. Comput. Vis.*, 2010, vol. 30, no. 2, pp. 2201–2208.
- [12] G. Buchsbaum, "A spatial processor model for object colour perception," *J. Franklin Inst.*, vol. 310, no. 1, pp. 1–26, Jul. 1980.
- [13] C. O. Ancuti, C. Ancuti, C. D. Vleeschouwer, and P. Bekaert, "Color balance and fusion for underwater image enhancement," *IEEE Trans. Image Process.*, vol. 27, no. 1, pp. 379–393, Jan. 2018.
- [14] K. He, J. Sun, and X. Tang, "Single image haze removal using dark channel prior," *IEEE Trans. Pattern Anal. Mach. Intell.*, vol. 33, no. 12, pp. 2341–2353, Dec. 2011.
- [15] A. Galdran, D. Pardo, A. Picón, and A. Alvarez-Gila, "Automatic Red-Channel underwater image restoration," *J. Vis. Commun. Image Represent.*, vol. 26, pp. 132–145, 2015.
- [16] N. Carlevaris-Bianco, A. Mohan, and R. M. Eustice, "Initial results in underwater single image dehazing," in *Proc. IEEE OCEANS Conf.*, 2010, vol. 27, no. 3, pp. 1–8.
- [17] P. Drews-Jr, E. D. Nascimento, F. Moraes, S. Botelho, M. Campos, and R. Grande-Brazil, "Transmission estimation in underwater single images," in *Proc. IEEE Int. Conf. Comput. Vis.*, Dec. 2013, pp. 825–830.
- [18] Y. T. Peng, X. Zhao, and P. C. Cosman, "Single underwater image enhancement using depth estimation based on blurriness," in *Proc. IEEE Int. Conf. Image Process.*, 2015, pp. 4952–4956.
- [19] Y. T. Peng and P. C. Cosman, "Underwater image restoration based on image blurriness and light absorption," *IEEE Trans. Image Process.*, vol. 26, no. 4, pp. 1579–1594, Apr. 2017.
- [20] Y. T. Peng and P. C. Cosman, "Single image restoration using scene ambient light differential," in *Proc. IEEE Int. Conf. Image Process.*, 2016, pp. 1953–1957.
- [21] C. Li, J. Guo, S. Chen, Y. Tang, Y. Pang, and J. Wang, "Underwater image restoration based on minimum information loss principle and optical properties of underwater imaging," in *Proc. IEEE Int. Conf. Image Process.*, 2016, pp. 1993–1997.
- [22] S. Emberton, L. Chittka, and A. Cavallaro, "Hierarchical rank-based veiling light estimation for underwater dehazing," in *Proc. Brit. Mach. Vis. Conf.*, Sep. 2015, vol. 125, pp. 1–12.
- [23] C. Ancuti, C. O. Ancuti, C. D. Vleeschouwer, R. Garcia, and A. C. Bovik, "Multi-scale underwater descattering," in *Proc. Int. Conf. Pattern Recognit.*, 2017, pp. 4202–4207.
- [24] T. Dickey, M. Lewis, and G. Chang, "Optical oceanography: recent advances and future directions using global remote sensing and in situ observations," *Rev. Geophys.*, vol. 44, no. 1, 2006, Art. no. RG1001.
- [25] H. M. Dierssen and K. Randolph, "Remote sensing of ocean color," in *Earth System Monitoring*. New York, NY, USA: Springer, 2013, pp. 439–472.
- [26] J. Breneman, H. Blasinski, and J. Farrell, "The color of water: Using underwater photography to estimate water quality," in *Proc. SPIE*, vol. 9023, no. 1, pp. 11, 2014.
- [27] B. L. McGlamery, "A computer model for underwater camera systems," *Ocean Opt.*, vol. 208, pp. 221–232, 1980.
- [28] S. Ghosh, R. Ray, S. R. K. Vadali, and S. N. Shome, "Light-particle interaction in underwater: A modified PSF," in *Proc. IEEE Int. Conf. Commun. Sign.*, 2014, pp. 1557–1562.
- [29] K. Wang, E. Dunn, J. Tighe, and J. M. Frahm, "Combining semantic scene priors and haze removal for single image depth estimation," in *Proc. IEEE PAMI-TC Premier Meeting Appl. Comput. Vis. (WACV)*, Mar. 2014, pp. 800–807.
- [30] M. Yang, A. Sowmya, Z. Wei, and B. Zheng, "Inshore eutrophic underwater image enhancement based on light-particles interaction descattering," in *Proc. MTS/IEEE OCEANS Conf.*, Aberdeen, Scotland, 2017, doi: [10.1109/OCEANSE.2017.8084657](https://doi.org/10.1109/OCEANSE.2017.8084657).
- [31] E. H. Land and J. J. McCann, "Lightness and retinex theory," *J. Opt. Soc. Amer.*, vol. 61, no. 1, pp. 1–11, 1971.

- [32] E. H. Land, "The retinex," *Amer. Sci.*, vol. 52, no. 2, pp. 247–253 and 255–264, 1964.
- [33] E. H. Land, "The retinex theory of color vision," *Sci. Amer.*, vol. 237, no. 6, pp. 108–128, Dec. 1977.
- [34] D. J. Jobson, Z. U. Rahman, and G. A. Woodell, "Properties and performance of a center/surround Retinex," *IEEE Trans. Image Process.*, vol. 6, no. 3, pp. 451–462, Mar. 1997.
- [35] D. J. Jobson, Z. U. Rahman, and G. A. Woodell, "A multiscale retinex for bridging the gap between color images and the human observation of scenes," *IEEE Trans. Image Process.*, vol. 6, no. 7, pp. 965–976, Jul. 1997.
- [36] Z. U. Rahman, D. J. Jobson, and G. A. Woodell, "Retinex processing for automatic image enhancement," *J. Electron. Imag.*, vol. 13, no. 1, pp. 100–110, 2004.
- [37] J. McCann, "Lessons learned from mondrians applied to real images and color gamuts," in *Proc. IS&T/SID 7th Color Imag. Conf.*, 1999, pp. 1–8.
- [38] R. Kimmel, M. Elad, D. Shaked, R. Keshet, and I. Sobel, "A variational framework for Retinex," *Int. J. Comput. Vis.*, vol. 52, no. 1, pp. 7–23, 2003.
- [39] M. K. Ng and W. Wang, "A total variation model for Retinex," *SIAM J. Imag. Sci.*, vol. 4, no. 1, pp. 345–365, 2011.
- [40] A. Levis, Y. Y. Schechner, and A. B. Davis, "Multiple-scattering micro-physics tomography," in *Proc. IEEE Conf. Comput. Vis. Pattern Recognit.*, 2017, pp. 5797–5806.
- [41] T. Johnsen, H. A. Bouman, S. Sathyendranath, and E. Devred, "Regional-scale changes in diatom distribution in the humboldt upwelling system as revealed by remote sensing: implications for fisheries," *ICES J. Mar. Sci.*, vol. 68, no. 4, pp. 729–736, 2011.
- [42] T. J. Li, *China Offshore Ocean: Ocean Optical Properties and Remote Sensing*. Beijing, China: Ocean Press, 2012, pp. 134–162.
- [43] A. Bricaud, A. Morel, and L. Prieur, "Absorption by dissolved organic matter of the sea (yellow substance) in the UV and visible domains," *Limnol. Oceanogr.*, vol. 26, no. 1, pp. 43–53, 1981.
- [44] J. T. O. Kirk, *Light and Photosynthesis in Aquatic Ecosystems*, 3rd ed., Cambridge, U.K.: Cambridge Univ. Press, 2011.
- [45] C. L. Gallegos, D. L. Correll, and J. W. Pierce, "Modeling spectral diffuse attenuation, absorption, and scattering coefficients in a turbid estuary," *Limnol. Oceanogr.*, vol. 35, no. 7, pp. 1486–1502, 1990.
- [46] X. Fu, Y. Liao, D. Zeng, Y. Huang, X. Zhang, and X. Ding, "A probabilistic method for image enhancement with simultaneous illumination and reflectance estimation," *IEEE Trans. Image Process.*, vol. 24, no. 12, pp. 4965–4977, Dec. 2015.
- [47] T. Goldstein and S. Osher, "The split bregman method for L1-regularized problems," *Soc. Ind. Appl. Math.*, vol. 2, no. 2, pp. 323–343, 2009.
- [48] K. He, J. Sun, and X. Tang, "Guided image filtering," *IEEE Trans. Pattern Anal. Mach. Intell.*, vol. 35, no. 6, pp. 1397–1409, Jun. 2013.
- [49] M. Yang and A. Sowmya, "An underwater color image quality evaluation metric," *IEEE Trans. Image Process.*, vol. 24, no. 12, pp. 6062–6071, Dec. 2015.
- [50] Imatest. [Online]. Available: <http://www.imatest.com/>, Accessed on: Jan. 3, 2015.
- [51] R. J. Davies-Colley, "Measuring water clarity with a black disk," *Limnol. Oceanogr.*, vol. 33, no. 4, pp. 616–623, 1988.



**Miao Yang** (M'12) was born in Wu Chang City, China, in 1978. She received the B.S. and M.S. degrees in electronic engineering from Lanzhou University, Lanzhou, China, in 2004, and the Ph.D. degree in information science and engineering from the Ocean University of China, Qingdao, China, in 2009.

From 2010 to 2013, she was a Postdoctoral Fellow with Internet of Things Engineering Department, Jiangnan University, Wuxi, China. Since 2009, she has been a Professor with the Electronic Engineering Department, HuaiHai Institute of Technology. She is currently with Qingdao National Laboratory of Marine Science and Technology in underwater image understanding. She has authored more than 30 articles and holds two patents. Her research interests include underwater vision, image processing, computer vision, and 3-D reconstruction.



**Arcot Sowmya** (M'xx) received the Ph.D. degree in computer science from Indian Institute of Technology Bombay, Mumbai, India, in addition to other degrees in mathematics and computer science.

She is currently a Professor with the School of Computer Science and Engineering, University of New South Wales, Sydney, NSW, Australia. Her areas of research include learning in vision for segmentation and object recognition, as well as embedded system design. Her research has been applied to extraction of linear features in remotely sensed images as well as feature extraction, recognition, and computer aided diagnosis in medical images.



**Zhiqiang Wei** received the B.S. degree from Shandong University, Jinan, China, in 1992, the M.S. degree from Harbin Institute of Technology, Harbin, China, in 1995, and the Ph.D. degree from Tsinghua University, Beijing, China, in 2001.

He is currently a Professor with the Ocean University of China, Qingdao, China. His current research interests are in the fields of intelligent information processing, intelligent computing of ocean big data, and multimedia content analysis and understanding.



**Bing Zheng** received the B.A. degree in electronics and information system, the M.S. degree in oceanophysics, and the Ph.D. degree in computer application from the Ocean University of China, Qingdao, China, in 1991, 1995, and 2013, respectively.

He is currently a Professor with the Institute of Information Science and Engineering, Ocean University of China. And he is the head of the electronics department of Ocean University of China. His research interests are in the areas of underwater vision detection.